J. Fluid Mech. (1968), *vol.* 33, *part* 4, *pp.* 721–738
Prtnted in Great Britain

Flow of stratified fluid through curved screens

By Y. L. LAU† AND W. D. BAINES
Department of Mechanical Engineering, University of Toronto

(Received 9 February 1968)

A curved screen placed across a two-dimensional channel causes the streamlines to be deflected on passing through because of the variation in pressure drop across the section and the refraction effect at the screen. Uniform flows far upstream and far downstream are required by the boundary conditions. An analytical description is based on the separation of the field into two regions distant from the screen in which viscosity and molecular diffusion are negligible, plus a thin layer along the screen in which energy loss and streamline deflexion are concentrated. These are described by empirical relationships. For linear velocity and density distribution upstream of the screen, equations can be simplified so that algebraic relationships between the variables at the screen surface are obtained. These have been solved numerically for the shape of screen required to produce a specified velocity distribution. An approximate solution is also obtained for general velocity profiles and the screen shape which produces uniform shear is derived. Experimental verification of the analysis is obtained from measurements of the velocity and temperature distributions downstream of the derived screen shapes mounted in a wind tunnel 45·6 cm square.

It is also shown that the boundary layers along a tunnel wall are accelerated or retarded by the screen depending on the loss coefficient. This effect is evident in all observations.

The case of homogeneous fluid is described by a simplified version of the analysis and several examples of velocity distributions are produced. These are verified by experiment and compared with those predicted by Elder (1959).

1. Introduction

A screen placed in a flow field causes deflexion of the streamlines towards the normal to the screen as they pass through, in a similar way to the refraction of light at a material interface. This is distinct from the pressure drop across the screen produced by the wakes of the elements. Schubauer, Spangenberg & Klebanoff (1950) revealed that the pressure drop is uniquely related to the solidity of the screen and the velocity component normal to it. They also found that the deflexion of the streamlines depended only upon the resistance coefficient of the screen defined as the ratio of the pressure drop to the kinetic energy of the velocity normal to the screen. For a curved screen placed in a flow in which the upstream velocity is uniform, the streamlines from top to bottom will be incident upon the screen at different angles. The pressure drop thus varies across the

† Present address; Hydraulics Laboratory, National Research Council, Ottawa, Canada.

section, inducing a lateral flow, and the refraction effect adds to it. As a result, the flow field downstream of the screen will not have the same velocity distribution. Conceivably, a screen could be shaped to produce the proper energy loss and deflexion of streamlines so that a uniform flow, after passing through the screen, becomes a flow with some prescribed velocity distribution. Shear flows with constant vorticity or boundary-layer-type velocity profiles could then be produced by means of curved screens placed in a wind tunnel. These have wide engineering applications in the simulation of meteorological and hydrological motions. Many of these flows occur in a fluid which is density stratified. In this paper the stratification of a flow passing through a screen will be considered and experiments described which verify the analytical solution.

In recent years there have been extensive applications of screens in the production of specified velocity profiles. Owen & Zienkiewicz (1957) produced a linear profile in a homogeneous fluid by means of rods placed in the plane normal to the incident stream, but this involved the careful spacing of numerous rods at varying distances apart. It is not very efficient because slight variations in spacing produce large velocity changes and an inherently non-uniform turbulence field is produced which tends to smooth the profile. Elder (1959) considered curved screens and obtained a relationship between the shape of the screen and the upstream and downstream velocity profiles. This analysis was based on linearized equations and was verified for small streamline deflexions. However, the screen shape designed to produce a linear velocity profile did not do so. The reason is outlined in appendix A.

2. Solution of the streamfunction

In the analysis given here, the solutions of the streamfunction upstream and downstream of the screen are matched at the screen. An approximation is made which enables the unknown constants in the solutions to be determined. An energy relationship is then used to predict the screen shape.

2.1. *Flow field far from screen*

Consider the steady, two-dimensional flow of a non-homogeneous, incompressible fluid in a channel which has a screen of arbitrary shape placed across it. The effects of viscosity and molecular diffusivity are neglected everywhere except at the screen, where a dissipation of energy takes place. The flow fields upstream and downstream of the screen will thus be inviscid motions with density conserved.

Co-ordinate axes x and y are chosen, x being the direction parallel to the wall. A transformation introduced by Yih (1958) is used to simplify the equations of motion. Writing

$$u' = (\rho/\rho_0)^{\frac{1}{2}} u, \quad v' = (\rho/\rho_0)^{\frac{1}{2}} v, \quad \psi' = \int (\rho/\rho_0)^{\frac{1}{2}} d\psi,$$

in which ρ_0 is a reference density and u', v' and ψ' are the transformed velocities and streamfunction, the equation for ψ' is

$$\rho_0 \nabla^2 \psi' + gy \frac{d\rho}{d\psi'} = \frac{dH}{d\psi'}, \tag{1}$$

where $$\nabla^2 = \frac{\partial^2}{\partial x^2} + \frac{\partial^2}{\partial y^2} \quad \text{and} \quad H = p + \rho \frac{u^2+v^2}{2} + \rho g y;$$

variables without a prime refer to the physical field.

This equation is valid either upstream or downstream of the screen although $dH/d\psi'$ will generally be different for the two regions.

2.2. *Upstream solution*

For simplicity, attention is restricted to the case in which the upstream density variation is linear and the upstream velocity u' constant. Far upstream, conditions are designated by the subscript $-\infty$, whence

$$u'_{-\infty} = u_0 \text{ (a constant)}, \quad \rho_{-\infty} = \rho_0(1-\beta y),$$

where $\beta = (\rho_0 - \rho_1)/h$; ρ_0, the reference density, is the density at the bottom of the channel, $y = 0$; and ρ_1 is the density at $y = h$, the height of the channel. Therefore

$$\left(\frac{d\rho}{d\psi'}\right)_{-\infty} = -\frac{\rho_0 \beta}{u_0}, \quad \left(\frac{dH}{d\psi'}\right)_{-\infty} = -\frac{\rho_0 g \beta}{u_0^2} \psi'_{-\infty}.$$

Equation (1) becomes

$$\nabla^2 \psi' + \frac{g\beta}{u_0^2} \psi' = \frac{g\beta}{u_0} y, \tag{2}$$

with boundary conditions

$$\psi' = 0 \quad \text{at} \quad y = 0, \qquad \psi' = u_0 h \quad \text{at} \quad y = h, \qquad \psi' = u_0 y \quad \text{at} \quad x = -\infty.$$

Non-dimensional variables are introduced by writing

$$U' = \frac{u'}{u_0}, \quad V' = \frac{v'}{u_0}, \quad \Psi = \frac{\psi'}{u_0 h}, \quad \xi = \frac{x}{h}, \quad \eta = \frac{y}{h}.$$

Equation (2) then becomes

$$\frac{\partial^2 \Psi'}{\partial \xi^2} + \frac{\partial^2 \Psi'}{\partial \eta^2} + F^{-2} \Psi' = F^{-2} \eta, \tag{3}$$

where $F = u_0/h(g\beta)^{\frac{1}{2}}$ is the Froude number of the flow.
The boundary conditions are

$$\Psi' = 0 \quad \text{at} \quad \eta = 0, \qquad \Psi' = 1 \quad \text{at} \quad \eta = 1, \qquad \Psi' = \eta \quad \text{at} \quad \xi = -\infty.$$

The solution of (3) has been given by Yih (1962) as

$$\Psi' = \eta + \sum_{n=1}^{\infty} B_n \exp\{(n^2\pi^2 - F^{-2})^{\frac{1}{2}} \xi\} \sin n\pi\eta \quad (\xi \leqslant 0). \tag{4}$$

It can be noted that the three boundary conditions given above are insufficient for the complete solution of Ψ'. The constants B_n can be obtained only when the solution is matched with the downstream one at the screen.

This solution violates the condition at $x = -\infty$ if $F < 1/\pi$, in which case waves are predicted which extend back to infinity. However, a Froude number of less than $1/\pi$ can only be obtained with very slow flows in a fluid with a high

density gradient. In wind-tunnel studies, practical considerations mean that the value of F is always far in excess of $1/\pi$. The case of $F < 1/\pi$ is not considered in this paper.

2.3. *Downstream solution for a linear case*

It will be assumed that there is negligible mixing at the screen so that $d\rho/d\psi'$ is the same function both upstream and downstream. The function $dH/d\psi'$ will be different from that upstream and for most velocity distributions $dH/d\psi'$ are non-linear functions of ψ' and the governing equation will be non-linear. However it can be seen that, if, at $x = +\infty$,

$$U'_{+\infty} = \frac{C}{u_0} + \frac{Gh}{\rho_0 u_0}\eta + \frac{F^{-2}}{2}\eta^2,$$

where G and C are constants, $(dH/d\psi')_{+\infty} = G$. With a density gradient attainable in wind-tunnel studies of say, 1 deg F/in. and a typical velocity of 20 ft./sec in a tunnel 2 ft. high, F^{-2} is approximately 0·006. The term $\frac{1}{2}F^{-2}\eta^2$ is thus small and the solution for the case of $(dH/d\psi')_{+\infty} = G$ will therefore be for a flow which is, in practice, linear far downstream.

The governing equation, after substitution of $dH/d\psi' = G$ and introduction of non-dimensional variables, is

$$\frac{\partial^2\Psi''}{\partial\xi^2} + \frac{\partial^2\Psi''}{\partial\eta^2} - F^{-2}\eta = \frac{Gh}{\rho_0 u_0}, \tag{5}$$

with boundary conditions

$$\Psi'' = 0 \quad \text{at} \quad \eta = 0, \qquad \Psi' = 1 \quad \text{at} \quad \eta = 1,$$

$$\Psi' = \frac{F^{-2}}{6}\eta^3 + \frac{Gh}{\rho_0 u_0}\frac{\eta^2}{2} + \frac{C}{u_0} \quad \text{at} \quad \xi = +\infty.$$

The solution is

$$\Psi' = \frac{F^{-2}}{2}\eta^3 + \frac{Gh}{\rho_0 u_0}\frac{\eta^2}{2} + \frac{C}{u_0} + \sum_{n=1}^{\infty} D_n \exp(-n\pi\xi)\sin n\pi\eta \quad (\xi \geqslant 0). \tag{6}$$

As is the case with the upstream solution, the constant D_n can be evaluated when conditions at the screen are considered.

2.4. *Solution for other downstream velocity profiles*

In the previous sections, two cases in which $dH/d\psi'$ is linear have been investigated. The only other linear case, $dH/d\psi' = a + b\psi'$, results in a velocity distribution of exponential form. For any other velocity distribution $U'_{+\infty}$, $(dH/d\psi')_{+\infty}$ is non-linear and will be difficult to solve. Therefore another method of solution for the flow downstream will have to be sought.

The vorticity equation is

$$\frac{D\Omega'}{Dt} = -\frac{g}{\rho_0}\frac{\partial\rho}{\partial x}, \tag{7}$$

where $\Omega' = (\partial v'/\partial x - \partial u'/\partial y)$ is the vorticity of the transformed flow. In this study, the density change in the y-direction is not large and in the absence of

excessively large deflexion of the streamlines, $\partial\rho/\partial x$ will be very small. One can then write $D\Omega'/Dt = 0$ without being very much in error. This means that the vorticity of the transformed flow is constant along a streamline and is equal to the vorticity at infinity. Then one can write $\Psi'' = \Psi''_{\pm\infty} + \Psi'^*$, where Ψ'^* is a perturbation streamfunction which does not add vorticity to the flow.
Therefore $\nabla^2\Psi'^* = 0$ with

$$\partial\Psi'^*/\partial\xi = 0 \quad \text{at} \quad \eta = 0 \quad \text{and} \quad \eta = 1.$$

This gives
$$\Psi''(\pm\xi) = \Psi''_{\pm\infty} + \sum_{n=1}^{\infty} A_n \exp(\mp n\pi\xi)\sin n\pi\xi. \tag{8}$$

It can be seen that the formal solution for the case $dH/d\psi' = G$ can be obtained by putting the corresponding $\Psi_{+\infty}$ into (8). This suggests that the assumption made concerning the preservation of Ω' is not inappropriate.

3. Conditions at the screen and solution of the screen profile

The following terms will be defined (see figure 1): θ = the angle between the normal to the screen at any point and the x-axis; $T = \tan\theta$; U'_n, U'_s = normal and tangential velocity components at the screen; $\eta_{-\infty}$, η_0, $\eta_{+\infty}$ = co-ordinate of a streamline far upstream, at the screen and far downstream. Subscripts 1 and 2 refer to variables upstream and downstream of the screen.

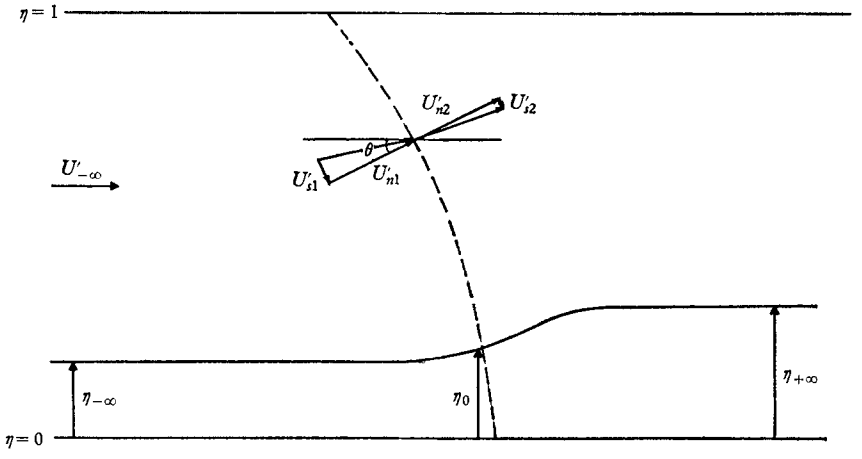

FIGURE 1. Definition sketch.

There are three conditions to be satisfied at the screen:

(i) For continuity requirements, the normal velocity component is conserved through the screen.

$U'_{n1} = U'_{n2}$ and from geometry this becomes

$$U'_1(\eta_0) = U'_2(\eta_0) - [V'_1(\eta_0) - V'_2(\eta_0)]T(\eta_0). \tag{9}$$

(ii) The ratio of the tangential velocities is a constant. For round bar wire screens it was found by Schubauer *et al.* (1950) that at small angles of incidence the tangential velocity component is changed by a factor $1{\cdot}1(1+K)^{-\frac{1}{2}}$, K being the resistance coefficient of the screen defined as

$$K = \frac{\Delta p}{\frac{1}{2}\rho u_n^2} = \frac{\Delta p}{\frac{1}{2}\rho_0 u_n'^2},$$

where Δp is the pressure drop across the screen. For any particular screen K is a constant at large screen Reynolds number.

Hence $U'_{s2}/U'_{s1} = 1{\cdot}1(1+K)^{-\frac{1}{2}} = 1-D$, where D is a constant for a particular screen.

This becomes

$$DU_1'(\eta_0)\,T(\eta_0) = V_2'(\eta_0) - V_1'(\eta_0)\,(1-D) - [V_1'(\eta_0) - V_2'(\eta_0)]\,T^2(\eta_0). \tag{10}$$

It can be seen that at either wall, where V' vanishes but not U', equation (10) is satisfied only if T is equal to zero. If the screen is not perpendicular to the wall, (10) can properly be applied only outside of a layer of thickness δ from the wall. δ has not been defined, but in the present experiments it is less than the thickness of the boundary layer.

(iii) There is energy loss only at the screen. The energy drop across the screen along any streamline is therefore equal to the difference between the energy on that streamline far upstream and far downstream.

Consider a streamline which is at height η_0 at the screen and at heights $\eta_{-\infty}$, $\eta_{+\infty}$ respectively far upstream and far downstream as shown in figure 1. Let the energy loss across the screen be equal to $\Delta H(\eta_0)$,

$$\begin{aligned}\Delta H(\eta_0) &= \Delta p + \tfrac{1}{2}\rho(U_{s1}^2 - U_{s2}^2)\\ &= \tfrac{1}{2}K\rho_0 U_n'^2 + \tfrac{1}{2}\rho_0(U_{s1}'^2 - U_{s2}'^2)\\ &= \tfrac{1}{2}\rho_0\cos^2\theta(\eta_0)[K(U_1'^2 + V_1'^2T^2 + 2U_1'V_1'T) + (V_1'^2 - V_2'^2)\\ &\qquad - 2T(U_1'V_1' - U_2'V_2') + (U_1'^2 - U_2'^2)T^2]_{\eta_0}.\end{aligned}$$

Subscript η_0 signifies that the quantities within the brackets are evaluated at $\eta = \eta_0$. Equating this with the energy difference at $-\infty$ and $+\infty$ gives

$$\begin{aligned}\cos^2\theta(\eta_0)[K(U_1'^2 + V_1'^2T^2 + 2U_1'V_1'T) + (V_1'^2 - V_2'^2) - 2T(U_1'V_1' - U_2'V_2')\\ + (U_1'^2 - U_2'^2)T^2]_{\eta_0}\\ = [U'^2(-\infty, \eta_{-\infty}) - U'^2(+\infty, \eta_{+\infty})] + \frac{2}{\rho_0 u_0^2}[p + \rho g h\eta]_{-\infty, \eta_{-\infty}}\\ - \frac{2}{\rho_0 u_0^2}[p + \rho g h\eta]_{+\infty, \eta_{+\infty}}.\end{aligned} \tag{11}$$

Equations (9), (10) and (11) are the three conditions from which the Fourier coefficients in the streamfunctions upstream and downstream and the screen inclination θ are to be solved.

The first simplification required is that the screen is at $x = 0$, which gives the velocities at the screen from equations (4) and (6),

$$U_1'(\eta_0) = 1 + \sum_{n=1}^{\infty} n\pi B_n \cos n\pi\eta_0,$$

$$V_1'(\eta_0) = -\sum_{n=1}^{\infty} (n^2\pi^2 - F^{-2})^{\frac{1}{2}} B_n \sin n\pi\eta_0,$$

$$U_2'(\eta_0) = \frac{F^{-2}}{2}\eta_0^2 + \frac{Gh}{\rho_0 u_0}\eta_0 + \frac{C}{u_0} + \sum_{n=1}^{\infty} n\pi D_n \cos n\pi\eta_0,$$

$$V_2'(\eta_0) = \sum_{n=1}^{\infty} n\pi D_n \sin n\pi\eta_0.$$

These are substituted into (9), (10) and (11), but brief inspection reveals that solution of these three equations will be very difficult. The Fourier coefficients B_n and D_n and the term T are non-linearly related. Equation (11) cannot be used until $\eta_{-\infty}$, η_0 and $\eta_{+\infty}$ can be related and this requires knowledge of B_n and D_n. It is clear that a further simplifying assumption has to be made.

3.1. *Simplifications for the solution*

It is assumed that the streamline pattern for the present case is much the same as if a screen normal to the flow is used to deflect the streamlines into the required downstream pattern. This enables equations (9) and (10) to be uncoupled from (11). Even though the values of U' and V' so calculated may not be exact, the errors involved when these are introduced into (11) will not be serious if the inclination of the screen, and hence T, is small. This is in fact compatible with the assumption that the velocities $U'(\eta_0)$ and $V'(\eta_0)$ are calculated at $x = 0$. Under the same assumption, terms involving $V'T$ and T^2 in (11) are also dropped. Equations (9), (10) and (11) are thus simplified to

$$U_1'(\eta_0) = U_2'(\eta_0), \tag{12}$$

$$(1-D)V_1'(\eta) = V_2'(\eta_0), \tag{13}$$

$$\cos^2\theta(\eta_0)[KU_1'(\eta_0) + V_1'(\eta_0) - V_2'^2(\eta_0)] = [U'^2(-\infty, \eta_{-\infty}) - U'^2(+\infty, \eta_{+\infty})] + \frac{2}{\rho_0 u_0^2}[p + \rho g h\eta]_{-\infty,\eta_{-\infty}} - \frac{2}{\rho_0 u_0^2}[p + \rho g h\eta]_{+\infty,\eta_{+\infty}}, \tag{14}$$

For the velocity profiles described in §§2.2 and 2.3, equations (12) and (13) become

$$1 + \sum_{n=1}^{\infty} n\pi B_n \cos n\pi\eta_0 = \frac{F^{-2}}{2}\eta_0^2 + \frac{Gh}{\rho_0 u_0}\eta_0 + \frac{C}{u_0} + \sum_{n=1}^{\infty} n\pi D_n \cos n\pi\eta_0$$

and

$$(1-D)\left[-\sum_{n=1}^{\infty} (n^2\pi^2 - F^{-2})^{\frac{1}{2}} B_n \sin n\pi\eta_0\right] = \sum_{n=1}^{\infty} n\pi D_n \sin n\pi\eta_0,$$

from which

$$B_n = \frac{2}{n\pi + (1-D)(n^2\pi^2 - F^{-2})^{\frac{1}{2}}} \frac{1}{n^2\pi^2} \frac{Gh}{\rho_0 u_0}[(-1)^n - 1] + \frac{(-1)^n}{n^3\pi^3} F^{-2} \tag{15}$$

and

$$D_n = -\frac{1-D}{n\pi}(n^2\pi^2 - F^{-2})^{\frac{1}{2}} B_n. \tag{16}$$

For a given η_0, $\eta_{-\infty}$ and $\eta_{+\infty}$ can now be calculated by equating the values of the streamfunction at the screen with those at infinity,

$$\eta_{-\infty} = \eta_0 + \sum_{n=1}^{\infty} B_n \sin n\pi\eta_0 = \frac{F^{-2}}{6}\eta_{+\infty}^3 + \frac{Gh}{\rho_0 u_0}\frac{\eta_{+\infty}^2}{2} + \frac{C}{u_0}\eta_{+\infty}. \tag{17}$$

Equation (14) becomes

$$\begin{aligned}\cos^2\theta(\eta_0)[KU_1'^2(\eta_0) + V_1'^2(\eta_0) - V_2'^2(\eta_0)] \\ = \left[U'^2(-\infty, \eta_{-\infty}) - \left(\frac{C}{u_0} + \frac{Gh}{\rho_0 u_0}\eta_{+\infty} + \frac{F^{-2}}{2}\eta_{+\infty}^2\right)^2\right] - F^{-2}\eta_{-\infty}^2 \\ + F^{-2}\left[F^{-2}\frac{\eta_{+\infty}^4}{4} + \frac{2}{3}\frac{Gh}{\rho_0 u_0}\eta_{+\infty}^3 + \frac{C}{u_0}\eta_{+\infty}^2\right] \\ + [KU'^2(0, 0) - U'^2(-\infty, 0) + U'^2(+\infty, 0)].\end{aligned} \tag{18}$$

In applying (18), the constant last term on the right-hand side has to be specified. This is accomplished by specifying the screen slope at the wall as $\theta = 0$. It is thereby assured that the deflexion equation is satisfied along the streamline $\eta = 0$. However, there is only one constant which can be specified and so the screen slope at $\eta = 1$ must be accepted at the value given by the analysis. Hence the velocity distribution produced may not be correct near $\eta = 1$.

The profile of the screen can be calculated by choosing a particular η_0, calculating $\eta_{-\infty}$ and $\eta_{+\infty}$ from (17) and then $\cos^2\theta(\eta_0)$ from (18). The process is repeated for various values of η from 0 to 1. With the screen position at the bottom as $x = 0$, the screen position at height η_0 is given by

$$\int_0^{\eta_0} T\, d\eta.$$

4. Experimental procedure

An experimental program was developed to verify the above analysis and, in particular, the assumptions made about the small screen slope and the effect of the screen on molecular transport.

The experiments were conducted in the heated wind tunnel of the Department of Mechanical Engineering, University of Toronto. The tunnel speed was approximately 20 ft./sec. Density stratification was produced by means of cylindrical rods placed across the tunnel, to which electrical power was supplied. Temperature in the tunnel was measured with a copper–constantan thermocouple. Mean velocity and pressure readings were made with total head and static pressure probes.

A removable test section was formed to the calculated screen profile and the screen mounted over it. This is inserted into the tunnel and measurements were then made at stations upstream and downstream. Lau (1966) provides further details regarding the experimental technique.

5. Discussion of cases tested

Several cases with different downstream and upstream velocity distributions were taken and the screen profiles were solved for and then tested. Tests were made on both stratified and homogeneous fluids; the latter are discussed in appendix A.

(i) The linear case of $dH/d\psi' = G$ was first tested. The mathematical model was

$$U'_{-\infty} = 1, \quad U'_{+\infty} = \frac{C}{u_0} + \frac{Gh}{\rho_0 u_0}\eta + \frac{F^{-2}}{2}\eta^2, \quad \rho_{-\infty} = \rho_0(1-\beta h\eta).$$

Two values of C/u_0 were arbitrarily chosen, so that the desired velocities were

$$U'_{+\infty} = 0{\cdot}95 + 0{\cdot}2\eta + 0{\cdot}0018\eta^2 \quad \text{and} \quad U'_{+\infty} = 0{\cdot}85 + 0{\cdot}3\eta + 0{\cdot}0018\eta^2.$$

This corresponded to the velocity $U_{+\infty}$ varying from 0·9 to 1·118 in the first case and from 0·85 to 1·168 in the other.

In calculating the streamfunctions and velocities, the series summation was taken from $n = 1$ to 120. Additional terms were found to produce negligible difference.

Figures 2 and 3 show the velocity profiles for these two tests. The results agree very well with theory. The only discrepancy appears inside the boundary layers as expected. For values of η between 0·075 and 0·85, the profiles are practically linear. Within the boundary layers there is a bulge in the downstream profile. This is due to the peculiar effect of the screen on a boundary-layer velocity distribution discussed in appendix B. The shear characteristics seem to remain fairly constant as the flow progresses.

The screen properties and profile for these cases are shown in table 1. Note that the screen is not normal to the wall at $\eta = 1$, which means that the deflexion equation (10) is not satisfied there. The streamlines near the top wall are still being deflected upward, but the wall effectively forces fluid back into the flow which contributes to the slightly bigger bulge at the top boundary layer.

Profiles of temperature distribution for these two cases are shown on figures 4 and 5. The verification of the predicted shape in the central region is again very good. In the boundary layers there is again a bulge resulting from the wall as discussed in the appendixes. It should be noted that the temperature distribution is dictated by the upstream and downstream velocity profiles and the upstream temperature owing to the assumption that density is conserved along streamlines. For this reason the temperatures θ_0 along the bottom wall and θ_1 along the top wall are the same on both sides of the screen. In the centre the deviation of the downstream profile from the one upstream (linear in this case) is a measure of the streamline deflexion. Relatively small deflexion was required to produce the 20 and 30 % velocity variation. This is the main reason why the verification is so good even though the screen slope is large, as shown in table 1.

(ii) Velocity profiles were chosen so that the governing equation was non-linear and the solution of §2.4 had to be used. The mathematical model was $U_{-\infty} = 1$ and $U_{+\infty} = (C/u_0) + b\eta$, which meant that $U'_{-\infty} = (1-\beta h\eta)^{\frac{1}{2}}$ and

$$U'_{+\infty} = \left[1 - \beta h\left(\frac{C}{u_0}\eta + \frac{b}{2}\eta^2\right)\right]^{\frac{1}{2}}\left(\frac{C}{u_0} + b\eta\right).$$

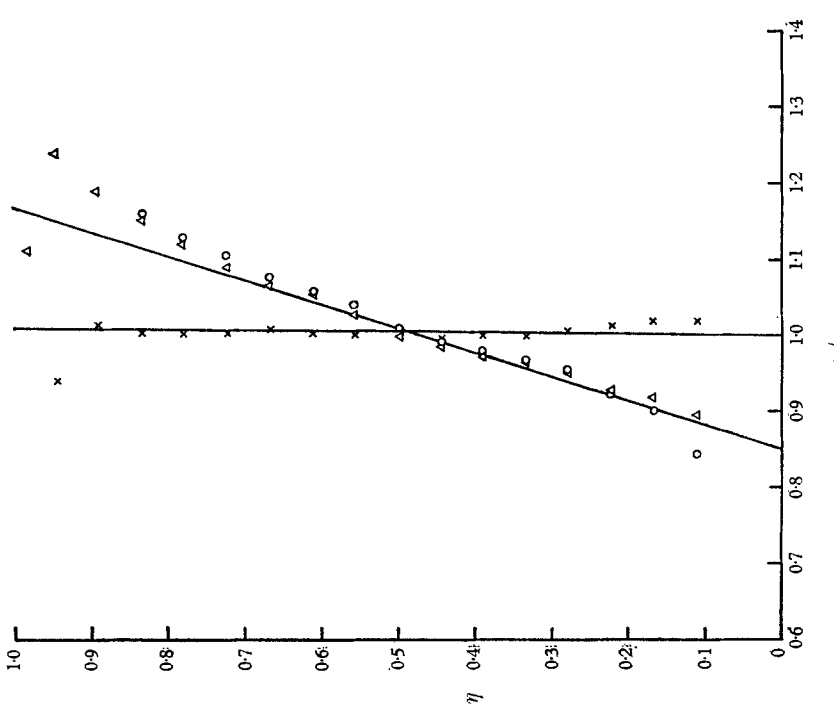

FIGURE 3. Velocity profile for a stratified flow with $dH/d\psi'$ constant. $U'_{+\infty} = 0{\cdot}85 + 0{\cdot}3\eta + 0{\cdot}0018\eta^2$, $u_0 = u$ at $\eta = 0{\cdot}47$. —, mathematical model; ×, $\xi = -2{\cdot}32$; △, $\xi = 2{\cdot}17$; ○, $\xi = 4{\cdot}82$.

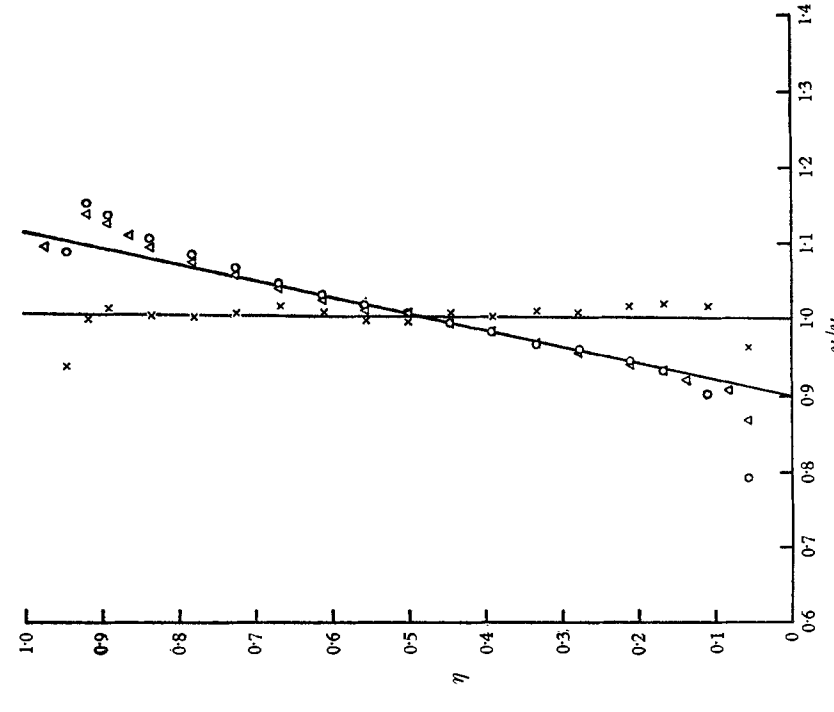

FIGURE 2. Velocity profile for a stratified flow with $dH/d\psi$ constant. $U'_{+\infty} = 0{\cdot}9 + 0{\cdot}2\eta + 0{\cdot}0018\eta^2$, $u_0 = u$ at $\eta = 0{\cdot}457$. —, mathematical model; ×, $\xi = -2{\cdot}32$; △, $\xi = 2{\cdot}17$; ○, $\xi = 4{\cdot}82$.

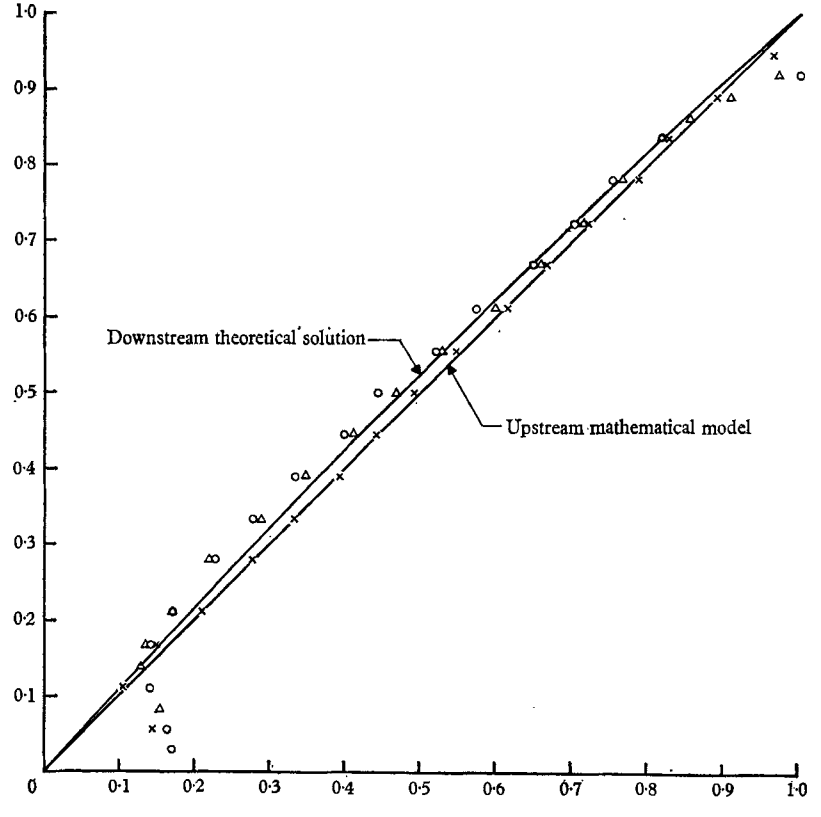

'IGURE 4. Theoretical and experimental temperature profiles for test of

$$U'_{+\infty} = 0{\cdot}9+0{\cdot}2\eta+0{\cdot}0018\eta^2.$$

$_0$ = temperature at $\eta = 0$; θ_1 = temperature at $\eta = 1$. ×, $\xi = -2{\cdot}32$; $\xi = 2{\cdot}17$; ○, $\xi = 4{\cdot}82$.

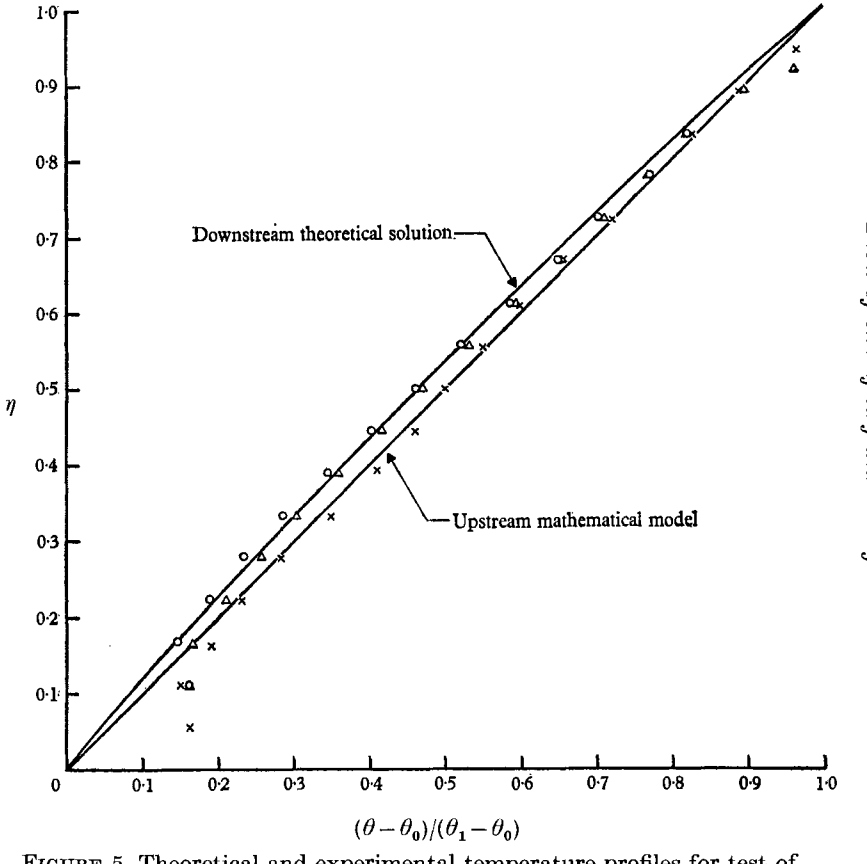

FIGURE 5. Theoretical and experimental temperature profiles for test of

$$U'_{+\infty} = 0{\cdot}85+0{\cdot}3\eta+0{\cdot}0018\eta^2.$$

θ_0 = temperature at $\eta = 0$; θ_1 = temperature at $\eta = 1$. ×, $\xi = -2{\cdot}32$; △, $\xi = 2{\cdot}17$; ○, $\xi = 4{\cdot}82$.

The results, shown on figures 6 and 7, indicate good agreement with theory. Bulges again are found in the boundary layers. The general shape of the screen is the same as the previous ones, normal to the wall at the bottom and curving with the concave side upstream so as to deflect all the streamlines upstream. For details of the screen profiles used, see Lau (1966).

Test no. 1. $U'_{-\infty} = 0{\cdot}9 + 0{\cdot}2\eta + 0{\cdot}0018\eta^2$, $\beta = 0{\cdot}02$		Test no. 2. $U'_{+\infty} = 0{\cdot}85 + 0{\cdot}30\eta + 0{\cdot}0018\eta^2$, $\beta = 0{\cdot}02$	
η	$\int T d\eta$	η	$\int T d\eta$
0·00	0·00	0·00	0·00
0·05	0·004	0·05	0·005
0·10	0·013	0·10	0·016
0·15	0·024	0·15	0·030
0·20	0·039	0·20	0·048
0·25	0·054	0·25	0·068
0·30	0·072	0·30	0·091
0·35	0·091	0·35	0·115
0·40	0·112	0·40	0·142
0·45	0·134	0·45	0·170
0·50	0·158	0·50	0·202
0·55	0·183	0·55	0·234
0·60	0·210	0·60	0·269
0·65	0·238	0·65	0·305
0·70	0·268	0·70	0·345
0·75	0·298	0·75	0·385
0·80	0·331	0·80	0·428
0·85	0·363	0·85	0·472
0·90	0·398	0·90	0·520
0·95	0·434	0·95	0·568
1·00	0·471	1·00	0·620

TABLE 1. Profile and properties of the screens tested for the case of a stratified flow with constant $dH/d\psi'$. Screen properties: 20 mesh, 0·016 in. diameter, solidity 0·538, $K = 2{\cdot}0$

These experiments have provided adequate proof that the analysis can be used to predict the flow through curved screens with small streamline deflexion and density variation. For even these cases large screen slopes are required if screens of low solidity are used. Note that $T > 1$ near $\eta = 1$ for both examples in table 1. Screens of large solidity ratio cannot be used in practical applications because of the instability discussed by Baines & Peterson (1951) and the effect on the boundary layer described in appendix B.

Appendix A. Application to homogeneous fluids

This analysis can be applied to the flow of a homogeneous fluid by setting $\beta = 0$ in all equations. No mathematical approximations are involved and the solution is not appreciably simpler than for a stratified fluid. Compared with the analysis of Elder (1959) it is much more complex and the screen shape calculation is more tedious. The essential difference between the two is the linear approxima-

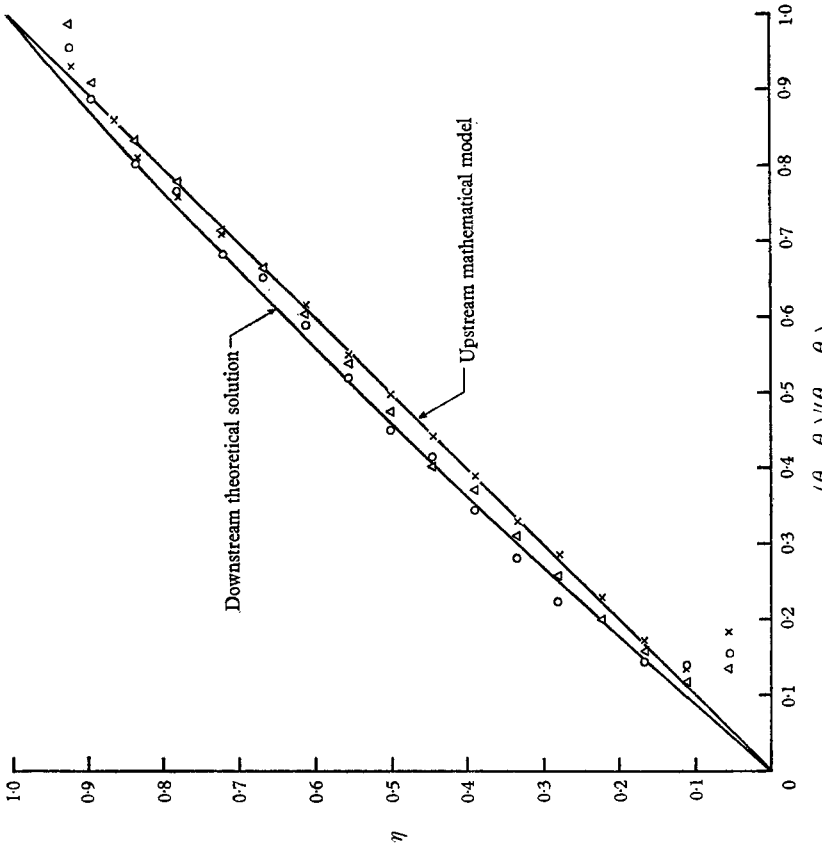

FIGURE 7. Theoretical and experimental temperature profiles for the test of $U_{+\infty} = 0{\cdot}85+0{\cdot}3\eta$.
θ_0 = temperature at $\eta = 0$; θ_1 = temperature at $\eta = 1$. ×, $\xi = -2{\cdot}32$; △, $\xi = 2{\cdot}17$; ○, $\xi = 4{\cdot}82$.

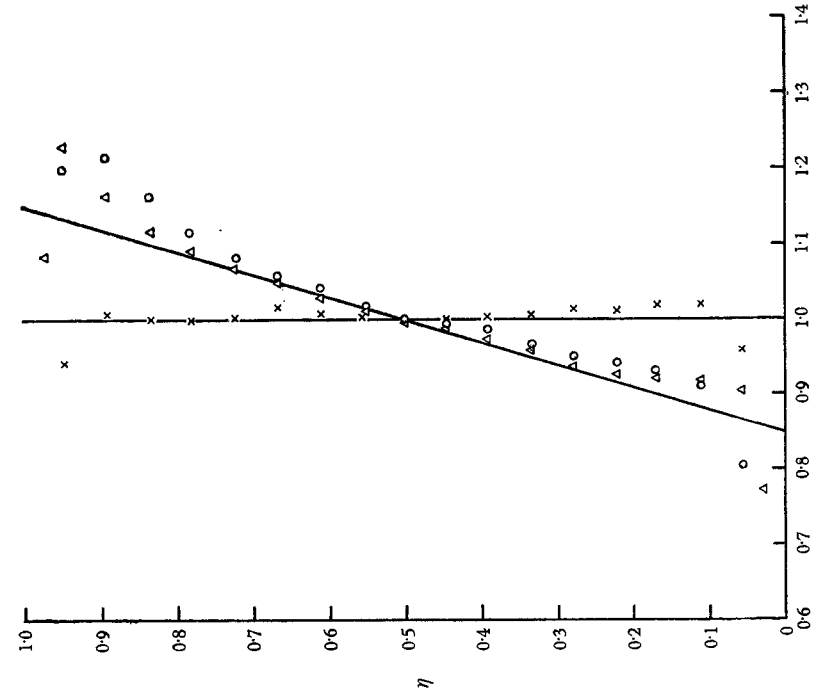

FIGURE 6. Stratified flow with a linear downstream velocity distribution. $U_{+\infty} = 0{\cdot}85+0{\cdot}3\eta$. —, mathematical model; ×, $\xi = -2{\cdot}32$; △, $\xi = 2{\cdot}17$; ○, $\xi = 4{\cdot}82$.

tion adopted by Elder for the energy loss equation (14). Elder assumed that for a screen the loss coefficient was constant for all y and that the velocity distributions everywhere differed from a constant velocity by a small amount. These assumptions appear to be too severe considering the large screen slope required in practice.

A comparison was made between the two analyses for flat sloping screens. These were mounted at angles of 10° and 24° to the normal to the flow. The measured velocity profile followed equally well both this analysis and that of Elder. However, for those small screen slopes all of the pertinent variables are small enough to be considered perturbations. This kind of comparison is not definitive but shows that in practice the analysis of Elder is preferred because of its simplicity.

The production of a constant shear flow from a constant upstream velocity was also studied. Screens were designed, using the above analysis, to produce velocity gradients $dU/d\eta$ of 0·3 and 0·5 respectively. These were constructed and the downstream velocity profiles measured. Agreement was the same as for the stratified flows shown on figure 6. Constant shear was produced over the central 80 % of the flow. In the boundary layer the same bulges were found.

A screen constructed following the analysis given in §7 and illustrated on figure 6 of Elder (1959) was found to produce an S-shaped velocity profile. This agreed with the constant shear equation over only the central 20 % of the flow. The reason for this lack of confirmation appears to be mainly due to the evaluation of Elder's equation (7.2) which in his notation is:

$$\frac{BE\pi^3}{\lambda}\frac{x'}{L} = 2\int_0^w \int_0^a \log\tan\tfrac{1}{2}t\,dt. \tag{A 1}$$

The function $\log\tan\frac{1}{2}t$ cannot be expanded in a Taylor series about $t = 0$ because of its limit value. Elder chose to expand it about $t = \frac{1}{2}\pi$, i.e. the duct centre line. If, however, the expansion of $\log\frac{1}{2}t\tan\frac{1}{2}t$ is considered, it is found possible to evaluate the integral in a straightforward manner. Integrating the result once gives the screen slope and a second integration gives the profile,

$$\frac{BE\pi^3}{\lambda}\frac{x}{L} = 4\left(\frac{w}{2}\right)^2\left[\log w - \tfrac{3}{2} + \frac{1}{18}\left(\frac{w}{2}\right)^2 + \frac{7}{1350}\left(\frac{w}{2}\right)^4 + \frac{31}{14\times 2835}\left(\frac{w}{2}\right)^6 + \frac{127}{45\times 18900}\left(\frac{w}{2}\right)^8 + \ldots\right]. \tag{A 2}$$

It can be shown directly from (A 1) that this profile is normal to both walls $w = 0$, $w = \frac{1}{2}\pi$ and is anti-symmetric about the centre line $w = \frac{1}{4}\pi$. In addition the slope near the centre line must be approximately linear because of the point of inflexion.

On figure 8 the shape given by (A 2) is compared with the one produced by this analysis for $\lambda = 0{\cdot}5$ using a screen with $K = 4{\cdot}2$. Over half of the section the shapes are virtually identical, but for the upper half which is the larger velocity region there is a significant difference. It is not unreasonable that the non-linear effects are greater for the larger velocity but rapid deviation of the shapes would not be expected from elementary considerations.

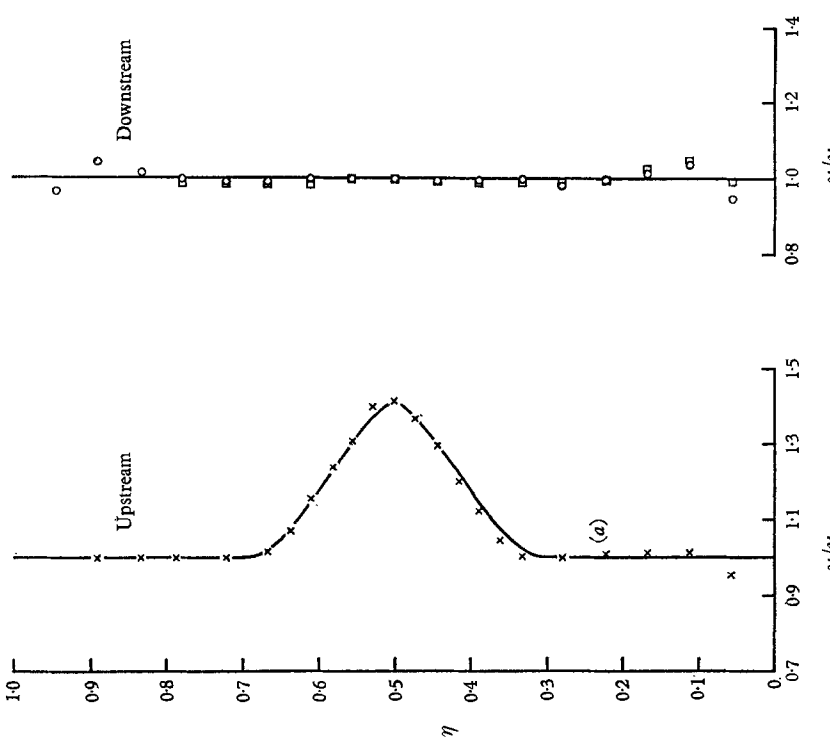

FIGURE 9. Correction of a non-uniform velocity profile with a screen. ×, $\xi = -2{\cdot}32$; □, $\xi = 3{\cdot}93$; ○, $\xi = 4{\cdot}82$.

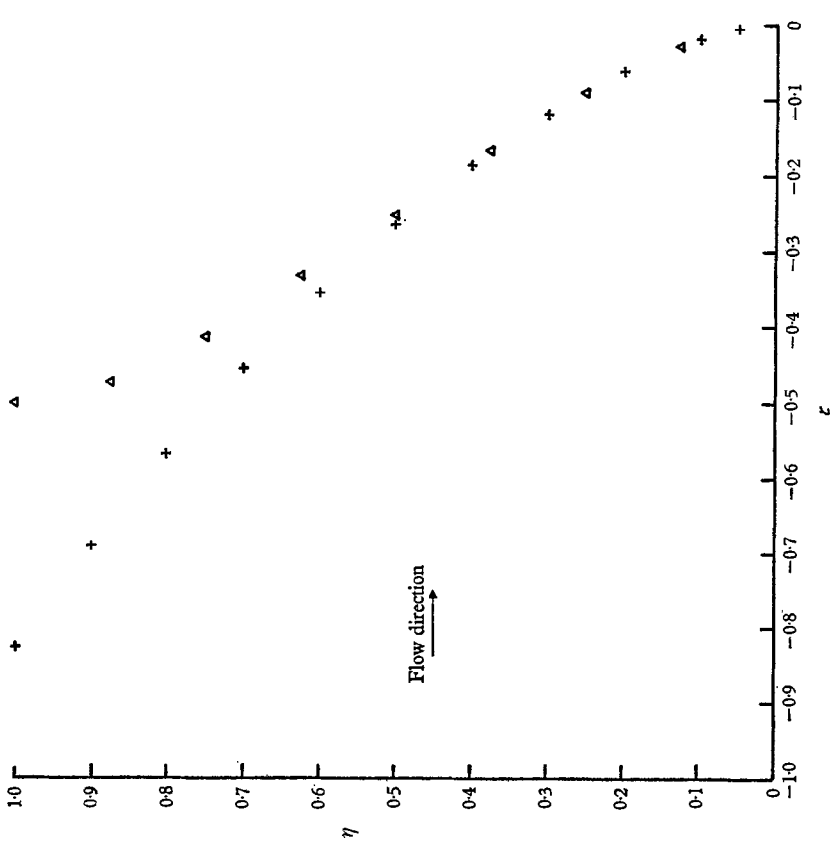

FIGURE 8. Screen shape required to produce linear velocity distribution $U = 0{\cdot}75 + 0{\cdot}5\eta$. +, Lau; △, Elder. (Based on $K = 4{\cdot}2$.)

Other velocity distributions were produced using this analysis to evaluate the practical applications. In one instance, a $\frac{1}{7}$-power law was produced from a uniform velocity distribution upstream. In another a large velocity excess was created by blocking most of the tunnel inlet except the central section. The maximum velocity was about 1·3 times the mean. A screen was designed to produce a constant velocity from this condition. In both of these cases the measured downstream profiles were as close to the desired one as would be expected. Figure 9 presents the results for the case of profile rectification.

Appendix B. Effect of screens on the velocity profile in the boundary layer

It was mentioned by Owen & Zienkiewicz (1957) that the velocity profiles they obtained departed from linearity near the walls. A bulge in the velocity profile appeared. Their explanation was that the fluid in the boundary layer, having a smaller velocity, suffered a smaller loss in total head than the fluid outside when passing through the screen. Hence the total head after the screen would increase towards the wall.

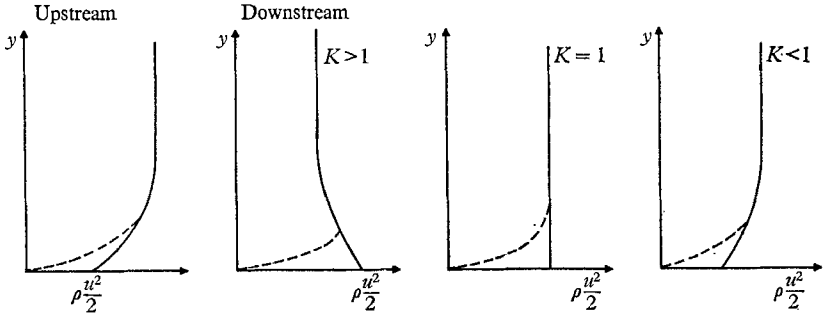

FIGURE 10. Kinetic energy distribution in the boundary layer behind a screen.

Even though cylindrical rods were used in their experiments, the same phenomenon can be expected when fluid flows through a screen. A simple analysis with the energy equation shows that this is indeed true except when K is less than or equal to one.

Consider a flow with a boundary-layer velocity profile approaching a screen. For simplicity, neglect density stratification and let the screen be normal to the plane of flow. The energy balance can be written as

$$\tfrac{1}{2}K\rho u^2(0,\eta_0) = \tfrac{1}{2}\rho[u^2(-\infty,\eta_{-\infty}) - u^2(+\infty,\eta_{+\infty})] + [p(-\infty,0) - p(+\infty,0)].$$

In the boundary layer, the streamlines are not subjected to large deflexions and $u^2(-\infty,\eta_{-\infty})$ is approximately equal to $u^2(0,\eta_0)$. Hence

$$\tfrac{1}{2}\rho u^2(+\infty,\eta_{+\infty}) \approx [p(-\infty,0) - p(+\infty,0)] - \tfrac{1}{2}(K-1)\rho u^2(-\infty,\eta_{-\infty}).$$

The kinetic energy downstream is then equal to the difference in static pressure at the wall, which does not vary with η, minus $(K-1)$ times the kinetic energy

upstream. Therefore, if $K > 1$, $u^2(+\infty, \eta_{+\infty})$ will be a maximum at the bottom and will decrease with y. If $K < 1$, the kinetic energy would increase with y and then become constant. These are shown qualitatively in figure 10, with the dotted line indicating the effect of shear stress.

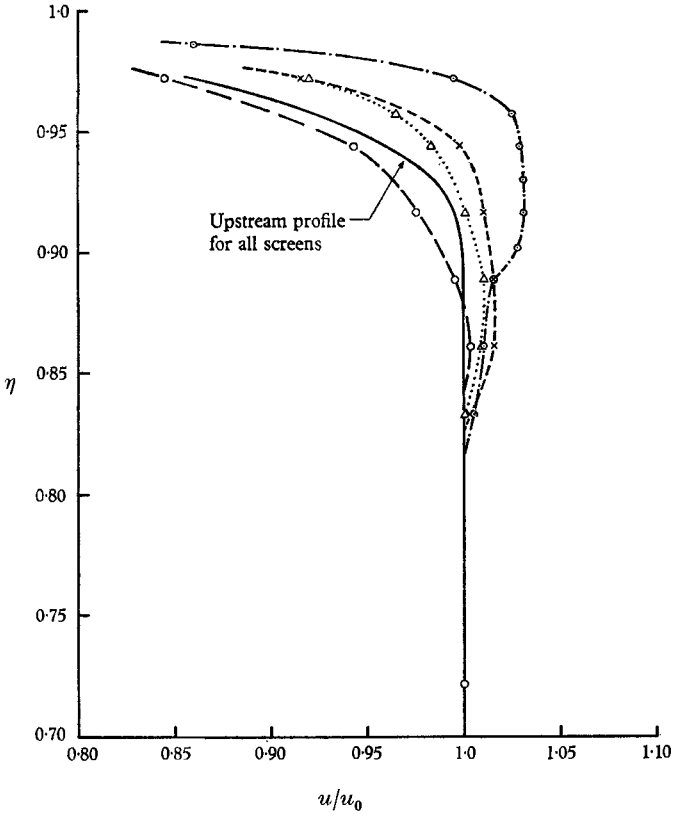

FIGURE 11. Effect of screen resistance coefficient on velocity distribution in the boundary layer. ⊙, $K = 4{\cdot}5$; ×, $K = 2{\cdot}4$; △, $K = 1{\cdot}5$; ○ = 0·97. All downstream measurements are for $\xi = 2{\cdot}32$.

Screens that are in common use generally have values of K greater than one. Therefore it can be expected that the artificially produced velocity distributions will have bulges near the walls which increase with the value of K used.

Screens with different K were inserted normal to the flow to check this effect. Screens of 18-mesh to 30-mesh with K varying from 0·97 to 4·2 were used. The velocity profiles are presented in figure 11. The result of the analysis is undoubtedly verified. With a screen having a K value of 0·97, the downstream velocity distribution shows no abnormality. However, with K values of 1·5, 2·43 and 4·5 respectively, increasingly larger velocity bulges appear. The exact location and size of the bulge cannot be determined by the present analysis since this involves the wall friction and shear stresses in the boundary layer.

These tests indicate that, as far as possible, screens with K value higher than 4 should not be used because of the big bulges produced in the boundary layer.

An attempt to produce a linear velocity distribution with a 40-mesh screen having a K of 4·2 was not as successful as the others because of the large bulge in the boundary layer. On the other hand, a screen with too small a K value would require excessively large curvature to produce the required deflexion. In general, a K value of 2 was found to be most satisfactory.

REFERENCES

BAINES, W. D. & PETERSON, E. G. 1951 *Trans. ASME* **73**, 467–77.

ELDER, J. W. 1959 *J. Fluid Mech.* **5**, 355–68.

LAU, Y. L. 1966 Ph.D. Thesis, University of Toronto.

OWEN, P. R. & ZIENKIEWICZ, H. K. 1957 *J. Fluid Mech.* **2**, 521–31.

SCHUBAUER, G. B., SPANGENBERG, W. G. & KLEBANOFF, P. S. 1950 *NACA TN* 2001.

YIH, C. S. 1958 *Proc. 3rd U.S. Nat. Congr. Appl. Mech.* pp. 857–61.

YIH, C. S. 1962 *Dynamics of Non-Homogeneous Fluids.* New York: MacMillan.

YIH, C. S., O'DELL, W. & DEBLER, W. R. 1958 *Proc. 4th U.S. Nat. Congr. Appl. Mech.* pp. 1441–53.